Electronic Structure, Properties, and Phase Stability of Inorganic Crystals: A Pseudopotential Plane-Wave Study

V. MILMAN,[1] B. WINKLER,[2] J. A. WHITE,[1] C. J. PICKARD,[3] M. C. PAYNE,[3] E. V. AKHMATSKAYA,[4] R. H. NOBES[4]

[1]*MSI, The Quorum, Barnwell Road, Cambridge CB5 8RE, United Kingdom*
[2]*Institut für Geowissenschaften, Mineralogie/Kristallographie, Olshausenstr 40, D 24098 Kiel, Germany*
[3]*TCM Group, Cavendish Laboratory, Cambridge University, Cambridge CB3 0HE, United Kingdom*
[4]*Fujitsu European Centre for Information Technology, 2 Longwalk Road, Stockley Park, Uxbridge UB11 1AB, United Kingdom*

Received 10 March 1999; accepted 1 September 1999

ABSTRACT: Recent developments in density functional theory (DFT) methods applicable to studies of large periodic systems are outlined. During the past three decades, DFT has become an essential part of computational materials science, addressing problems in materials design and processing. The theory allows us to interpret experimental data and to generate property data (such as binding energies of molecules on surfaces) for known materials, and also serves as an aid in the search for and design of novel materials and processes. A number of algorithmic implementations are currently being used, including ultrasoft pseudopotentials, efficient iterative schemes for solving the one-electron DFT equations, and computationally efficient codes for massively parallel computers. The first part of this article provides an overview of plane-wave pseudopotential DFT methods. Their capabilities are subsequently illustrated by examples including the prediction of crystal structures, the study of the compressibility of minerals, and applications to pressure-induced phase transitions. Future theoretical and computational developments are expected to lead to improved accuracy and to treatment of larger systems with a higher computational efficiency.
Int J Quant Chem 77: 895–910, 2000

Key words: density functional theory; pseudopotential; plane wave basis set; CASTEP

Correspondence to: V. Milman.

Introduction

During the past three decades, computational materials science has emerged as a new discipline in science and technology. It has deepened our fundamental understanding of materials and processes, has helped to interpret experimental data from diverse experimental techniques, and has opened exciting possibilities for the design of novel materials and processes by allowing quantitative property predictions.

While the enormous progress in computer technology was a necessary prerequisite for this development, it is probably safe to say that without density functional theory (DFT), the impact of computational materials science would have been substantially less significant. The aim of this article is to survey one particular DFT implementation that has been shown to be a highly productive tool for studies of complex solid-state systems, in particular inorganic crystals. The plane-wave pseudopotential (PW-PP) technique has become widely recognized as the method of choice for computational solid-state studies. The emphasis on the total energy and related properties makes PW-PP a technique that is ideally suited to structural studies based on a quantum-mechanical treatment of the electronic subsystem. This article discusses the major features of this approach and presents applications of PW-PP to such problems as the prediction of crystal structures, the study of the compressibility of minerals, and the investigation of pressure-induced phase transitions.

Methodology

DENSITY FUNCTIONAL THEORY AND CONVENTIONAL PSEUDOPOTENTIAL/PLANE-WAVE TECHNIQUES

It seems appropriate to start with a brief historical review of the approach. The formulation of DFT as a rigorous many-body approach by Hohenberg and Kohn [1] and Kohn and Sham [2] in the mid-1960s and the introduction of the local density approximation (LDA) represent major milestones. Subsequently, DFT evolved rapidly as the dominant approach in practical electronic structure calculations of solids and surfaces. In fact, there is no good alternative to DFT for accurate electronic structure calculations of metallic systems. The generalization of DFT to spin-polarized (magnetic) systems in the early 1970s [3, 4] paved the way for many impressive successes of this theory in the domain of magnetic materials. However, in the realm of molecular systems it took about two decades before DFT became generally accepted as a viable alternative to wave-function-based ab initio methods (such as Hartree–Fock and configuration interaction methods). Applications of the LDA to molecules and to molecule–solid interactions revealed a severe overestimation of binding energies, thus motivating improvements in the form of generalized gradient corrections (GGA) [5, 6].

A major challenge was to create a robust practical scheme for solving the DFT equations. PW-PP schemes have been used to study electronic structure of solids since the late 1950s (see [7] for a review). The main idea of the method is to simplify the DFT problem by considering only valence electrons. Core electrons are excluded under the assumption that their charge density is not affected by changes in the chemical environment. This approximation is well understood and gives a number of computational advantages:

- The pseudopotential is much weaker in the core region than the true Coulomb potential of the nucleus, and it does not have a singularity at the position of the nucleus.
- The resulting pseudo-wave functions are smooth and nodeless in the core region.
- Both pseudopotentials and pseudo-wave functions can be efficiently represented using a plane-wave basis set.
- Relativistic effects, which are mainly due to core electrons, can be included in the pseudopotential.
- Last but not least, there are fewer electronic states in the solid-state calculation.

The pseudopotential transferability is ensured by the norm-conservation condition, which guarantees that the pseudopotential is constructed in such a way that the charge contained in the core region of the pseudoatom is the same as that of the real atom.

The accurate representation of wave functions is an important part of the method. As a consequence of the Bloch theorem, the solution of the Kohn–Sham equations for a periodic system can be expanded in plane waves, which amounts to a three-dimensional Fourier series representation.

The convergence of this expansion is controlled by a single parameter, namely the highest frequency at which the series is terminated (conventionally defined as the highest kinetic energy of a plane wave). The control of the basis set convergence by a single parameter is a very appealing feature, particularly when compared with the tedious task of basis set improvements with Gaussians or other localized functions. Another major advantage is the ease of computing forces and stresses, which makes the PW-PP technique an efficient tool for structural studies. The plane waves are intimately linked to the pseudopotentials, since only pseudo-wave functions can be represented using a small number of Fourier components; an accurate expansion of all-electron wave functions would require an inordinate number of plane waves.

The original PW-PP schemes that were in use up to the early 1980s were based on diagonalization of the Hamiltonian matrix, and limitations of memory and computational speed restricted the maximum size of matrix that could be treated to the order of 1000. Whereas a minimum of 100 plane waves per atom is needed to represent the electronic orbitals in a total energy calculation of this kind, 10 atoms required at least 1000 plane waves, and thus represented the largest tractable system. These restrictions have certainly eased with the power of modern computing, but the primary reason that the total energy pseudopotential method has become so powerful is that the numerical methods used to solve the equations that determine the electronic state have changed completely.

ITERATIVE MINIMIZATION SCHEMES

The first changes in the way DFT equations are solved were suggested in 1985 by Car and Parrinello [8]. Their "molecular dynamics method" introduced three major ideas for speeding up calculations:

- The use of an iterative diagonalization instead of direct diagonalization of the Hamiltonian matrix.
- Overlapping the iterations toward self-consistency in the electronic potential with the iterations to determine the electronic wave functions.
- The use of fast Fourier transforms to reduce the computational cost and memory requirement for operating with the Hamiltonian on the electronic wave functions.

Combined, these ideas are central to the efficiency of modern total energy pseudopotential calculations. They provide a methodology in which computational cost scales linearly with the number of plane-wave basis states, removing the previous restriction on the number of atoms that could be treated. The new method allowed calculations to be performed on systems containing many tens of atoms. It also enabled the first ever dynamic simulations of ionic systems in which forces on atoms were correctly described via inclusion of the quantum mechanics of the electronic states.

The next step was to improve even further on the computational algorithm. It appeared that the particular iterative diagonalization technique introduced by Car and Parrinello [8] was not necessarily the most efficient, especially for metals and narrow-gap semiconductors. The conjugate gradient technique of relaxing the electronic configuration to its ground state is a more robust and efficient way to solve the DFT equations [7]. Simultaneous conjugate gradient update of all wave functions offers further advantages [9], albeit at a cost of increased memory requirements.

Considerable effort has gone into improving the pseudopotentials used. One drawback of pseudopotentials is that the ionic potential is angular-momentum dependent or "nonlocal," and it is computationally expensive to determine the angular momentum components of each electronic wave function around every atom. Techniques have been developed to optimize pseudopotentials [10, 11] to reduce the size of the plane-wave basis set. The Kleinman–Bylander scheme [12] uses a separable form of the potential to reduce the number of nonlocal projections that have to be performed. By performing these projections in real space and exploiting the finite range of the nonlocality around every atom, the computational cost associated with the use of nonlocal pseudopotentials has been further reduced [13].

Geometry optimization of complex structures with many degrees of freedom, including internal coordinates and cell parameters, is the main application area of the PW-PP technique. The BFGS approach [14] provides an efficient scheme for geometry optimization, either at ambient conditions or under applied external stress. An iterative update of the inverse Hessian, based on the quantum-mechanically calculated stress tensor and atomic forces, represents the most robust scheme within this framework. All these algorithmical develop-

ments have been available within the CASTEP computer code since the early 1990s [15].

It became obvious from even early applications of the method [7] that pseudopotential calculations worked extremely well for most atoms, including transition metals and first-row elements. The molecular dynamics method opened up completely new application areas. The robustness and accuracy of the PW-PP scheme enabled the study of such problems as the 7×7 reconstruction of the Si(111) surface [16, 17], the dynamics of dissociative chemisorption at semiconductor surfaces [18], the dissociative adsorption of small molecules on surfaces of metals and insulators [19–23], and the electronic and elastic properties of dislocations and characteristics of dislocation-point defect interaction [24–26]. The rapid increase in computing power made it possible to study such complex systems and processes as AFM (atomic force microscopy) imaging of reactive surfaces [27], scanning tunneling microscopy and scanning tunneling spectroscopy (STS) study of reconstructed surfaces of semiconductors [28], and mechanical polishing of diamond surfaces [29]. The area of structural studies of nonideal crystals currently includes such challenging applications as complex details of grain boundary structure [30], interaction of grain boundaries with impurities [31–34], and ultimately grain boundary sliding in materials with different types of interatomic bonding [35, 36].

The PW-PP studies of nonperiodic systems have been for some time confined to investigations of molecule–surface interactions, in particular, molecular adsorption on surfaces [18–23, 37–40] and chemical reactions in zeolites [41, 42]. It has, however, been shown that the plane-wave method can reproduce the accuracy of large Gaussian basis calculations for nonperiodic systems with a competitive computational time [43, 44]. Furthermore, a recent study of molecular polarizabilities of prototypical liquid crystal-forming molecules showed that the polarizability is generally overestimated by the localized basis methods and that the results do not necessarily converge with increasing localized basis set sophistication [45]. Further applications showed that the PW-PP approach can provide useful quantitative information on, e.g., conformational maps of medium-sized molecules [46, 47], activity of enzymes such as cytochrome P450 [48], and vibrational properties of molecules [49] and molecular crystals [50].

The PW-PP approach can be made more efficient for studies of molecular systems if one recognizes that the regions of low electron density in the computational supercell can be treated using fewer basis functions than the high-density ones. This can be technically achieved in the adaptive coordinate method suggested by Gygi [51]. This technique introduces a new set of basis functions that depend on a coordinate transformation and can adapt themselves to represent the solutions of the Kohn–Sham equation optimally. The adaptive coordinate method has been subsequently modified into an efficient tool for solid-state studies [52]. A further development of this approach led to the creation of a real-space adaptive coordinate method, which does not require a basis set, but uses the multigrid scheme within the finite-difference approach to solve the DFT equations numerically [53, 54].

The modeling of complex systems such as those described above usually involves the quantum-mechanical description of about 100 atoms, with the biggest cells containing around 500 atoms [17, 24]. Such calculations until recently required massively parallel supercomputers for which an efficient parallel implementation of the PW-PP methodology has been developed in the computer code CETEP, based on real and reciprocal space decomposition [55]. A similar and independent parallel version, FINGER, also provides an option of *k*-point parallelism [56]. However, a further algorithmic breakthrough was needed (i) to bring calculations for tens and hundreds of atoms to workstations and (ii) to extend the system size available to supercomputing applications, especially with respect to the length of molecular dynamics runs.

ULTRASOFT PSEUDOPOTENTIALS

Two major achievements have become available recently that greatly enhance the efficiency of the PW-PP technique: (i) routine use of ultrasoft pseudopotentials and (ii) the use of the density mixing scheme for solving the DFT equations in conjunction with the conjugate-gradient algorithm for wave functions. These developments, first made available as part of the VASP code [57], have recently been incorporated into the CASTEP program [15].

The idea of ultrasoft pseudopotentials as put forward by Vanderbilt [58] is that the relaxation of the norm-conserving condition can be used to generate much softer potentials, i.e., the basis set size can be made substantially smaller. In this scheme the pseudo-wave functions can be made softer within

the core region, so that the cutoff energy can be reduced dramatically. The pseudopotential transferability is maintained by introducing a generalized orthonormality condition. Then the electron density, given by the squared moduli of the wave functions, has to be augmented in the core region to recover the full electronic charge. The electron density is thus subdivided into a smooth part that extends throughout the unit cell and a hard part localized in the core regions. The augmented part appears in the density only, not in the wave functions. This differs from methods like linearized augmented plane wave technique (LAPW), where a similar approach is applied to wave functions.

The augmentation charges are normally "pseudized" to make calculations feasible. It has been rigorously proven [59] that without such pseudization, i.e., in the limit of very accurate augmentation charges, the ultrasoft pseudopotential method should—and in fact does—reproduce the results of the all-electron projector augmented wave method [60].

Ultrasoft potentials have another advantage in addition to being much softer than the norm-conserving potentials. The generation algorithm for ultrasoft potentials produces Kleinman–Bylander [12] separable potentials for more than one projector function in each angular momentum channel, which guarantees good scattering properties over a prespecified energy range. This results in much better transferability and accuracy of pseudopotentials. Ultrasoft potentials usually treat "shallow" core electrons as valence states by including multiple sets of occupied states in each angular momentum channel. This also adds to high accuracy and transferability of the potentials, although at a price of computational efficiency. Nonlinear core corrections can be used to describe shallow core states in a more approximate way if computational cost becomes an issue [61].

The ultrasoft pseudopotential formulation is more complex than the formalism for norm-conserving pseudopotentials. In particular, one has to solve a generalized eigenvalue problem as a result of using nonorthogonal wave functions. It follows that in the cases where the effect of reducing the basis set size is not large, the overall gain of the ultrasoft pseudopotential approach can be insignificant. The elements that can be described with sufficiently soft norm-conserving potentials (e.g., Al, Si) do not necessarily warrant ultrasoft pseudopotential treatment. On the other hand, ultrasoft potentials provide great improvements in both accuracy and computational cost for elements with the valence 1s, 2p, 3d, or 4f electrons where the norm-conserving potentials are necessarily quite hard.

DENSITY MIXING SCHEME

The density mixing scheme as described by Kresse and Furthmüller [57] presents the latest development of the robust stable algorithm for calculating the Kohn–Sham ground state within the PW-PP formalism. The main advantage of the density mixing scheme over the standard conjugate-gradient-based minimization [7] is that metallic systems can be reliably converged in a relatively small number of steps. The conjugate-gradient method can be extended to treat metallic systems efficiently if an all-bands approach is adopted, i.e., if all electronic bands are updated simultaneously. The density mixing method, however, can be incorporated easily into a band by band approach [7], which is more memory efficient. The direct inversion in the iterative subspace (DIIS) scheme proposed by Pulay [62] is used to mix input and output charge densities. Further additions specific to the PW scheme, such as the use of preconditioning and an optimized metric for evaluating the scalar products, make the scheme reliable and at the same time highly efficient [57]. The combination of ultrasoft potentials and the density mixing scheme leads to speedup factors of 5–10 for semiconducting and insulating systems and to factors of 15–30 for metallic systems when compared with the conjugate-gradient scheme with norm-conserving pseudopotentials.

The accuracy of ultrasoft potentials is illustrated by Table I. We performed geometry optimization for a number of relatively simple structures, some of them having a symmetry as low as monoclinic, and found that in practically all cases the calculated cell parameters agree to within 2% with the experimental values. In fact, in most cases the agreement was better than 1%, including compounds of transition metals and rare-earth elements. In other words, it is difficult to separate an error introduced by the use of pseudopotentials from the inherent error due to the use of DFT to describe exchange–correlation effects. The same degree of agreement with experiment was observed for a few molecular systems included in Table I.

To summarize, the state-of-the-art PW-PP techniques [15, 53] make accurate DFT calculations for periodic cells with tens and even hundreds of atoms routinely available on a workstation.

TABLE I

Calculated structural properties of various inorganic compounds and small molecules (cell parameters or molecular bond lengths in Å, cell angles, fractional coordinates of atoms). Space group numbers for crystalline systems are given according to [63].

Element	Compound (space group number)	Structural parameters			
		Experiment	Temperature and reference	CASTEP	Error (%)
Ag	Ag (225)	$a = 4.0857$	RT [64]	$a = 4.112$	0.6
	Ag_2O (224)	$a = 4.73$	RT [64]	$a = 4.788$	1.2
Al	Al (225)	$a = 4.0496$	RT [64]	$a = 3.965$	−2.0
	Al_2O_3 (167)	$a = 4.759$	RT [65]	$a = 4.703$	−1.2
		$c = 12.991$		$c = 12.871$	−0.9
Am	AmO (225)	$a = 4.960$	RT [66]	$a = 5.084$	+2.5
Ar	Ar (225)	$a = 5.256$	4 K [67]	$a = 5.256$	0.0
As	As (166)	$a = 3.760$	4 K [68]	$a = 3.705$	−1.5
		$c = 10.441$		$c = 10.083$	−3.4
		$\zeta = 0.22764$		$\zeta = 0.2313$	1.6
	GaAs (216)	$a = 5.653$	RT [64]	$a = 5.663$	0.2
Au	Au (225)	$a = 4.0783$	RT [64]	$a = 4.1528$	1.8
	$SrAu_2Si_2$ (139)	$a = 4.37$	RT [69]	$a = 4.437$	1.5
		$c = 10.14$		$c = 10.074$	−0.7
B	BN (216)	$a = 3.615$	RT [64]	$a = 3.598$	−0.5
	BCl_3 (173)	$a = 6.08$	108 K [70]	$a = 6.216$	2.2
		$c = 6.55$		$c = 6.632$	1.2
Ba	Ba (229)	$a = 5.019$	RT [71]	$a = 4.992$	−0.7
	BaO (225)	$a = 5.523$	RT [64]	$a = 5.562$	0.7
Be	Be (194)	$a = 2.2856$	RT [64]	$a = 2.279$	−0.3
		$c = 3.5832$		$c = 3.579$	−0.1
	BeO (186)	$a = 2.6979$	RT [72]	$a = 2.738$	1.5
		$c = 4.3772$		$c = 4.446$	1.6
	BeS (216)	$a = 4.855$	RT [64]	$a = 4.871$	0.3
Bi	BiOF (129)	$a = 3.7469$	RT [70]	$a = 3.633$	−3.0
		$c = 6.226$		$c = 6.267$	0.7
	LaBi (225)	$a = 6.57$	RT [64]	$a = 6.648$	1.2
	Bi_2O_3 (224)	$a = 5.45$	RT [73]	$a = 5.360$	−1.7
Br	Br_2	$a = 2.2811$	RT [64]	$a = 2.288$	0.3
	LiBr (225)	$a = 5.489$	RT [74]	$a = 5.467$	−0.4
C	Diamond (227)	$a = 3.556$	4 K [64]	$a = 3.539$	−0.5
	CO	d(C—O) = 1.1283	RT [64]	1.144	1.7
Ca	Ca (225)	$a = 5.5884$	RT [64]	$a = 5.506$	−1.5
	CaO (225)	$a = 4.797$	10 K [75]	$a = 4.817$	0.4
Cd	Cd (194)	$a = 2.9793$	RT [64]	$a = 3.035$	1.9
		$c = 5.6196$		$c = 5.665$	0.9
	CdSe (216)	$a = 6.05$	RT [64]	$a = 6.146$	1.6
Ce	CeS (225)	$a = 5.777$	RT [76]	$a = 5.772$	−0.1
	CeO_2 (225)	$a = 5.412$	RT [77]	$a = 5.455$	0.8
Cl	Cl_2	d(Cl—Cl) = 1.9878	RT [64]	1.990	0.0
	CsCl (221)	$a = 4.112$	RT [64]	$a = 4.167$	1.3
Co	ε-Co (194)	$a = 2.507$	RT [64]	$a = 2.481$	−1.0
		$c = 4.069$		$c = 4.018$	−1.2
	α-Co (225)	$a = 3.544$	700 K [64]	$a = 3.494$	−1.4
	$CoSi_2$ (225)	$a = 5.365$	RT [78]	$a = 5.300$	−1.2
Cr	Cr (229)	$a = 2.8846$	RT [64]	$a = 2.851$	−1.2
	Cr_3Si (223)	$a = 4.556$	RT [79]	$a = 4.525$	−0.7

(Continued)

TABLE I
(Continued)

Element	Compound (space group number)	Structural parameters: Experiment	Temperature and reference	CASTEP	Error (%)
Cs	Cs (229)	$a = 6.141$	RT [64]	$a = 6.14$	0.0
	CsH(225)	$a = 6.388$	RT [80]	$a = 6.387$	0.0
Cu	Cu (225)	$a = 3.6147$	RT [64]	$a = 3.631$	0.5
	Cu_2O (224)	$a = 4.267$	100 K [81]	$a = 4.253$	−0.3
Eu	EuS (225)	$a = 5.957$	RT [64]	$a = 5.957$	0.0
F	F_2	d(F—F) = 1.4119	RT [64]	1.418	−0.1
	CaF_2 (225)	$a = 5.447$	77 K [82]	$a = 5.496$	0.9
Fe	Fe (229)	$a = 2.8664$	RT [64]	$a = 2.883$	0.6
	$FeSi_2$(123)	$a = 2.684$	RT [70]	$a = 2.649$	−1.3
		$c = 5.128$		$c = 5.037$	−1.7
Ga	GaN (216)	$a = 4.50$	RT [64]	$a = 4.535$	0.8
	GaP (216)	$a = 5.4505$	RT [64]	$a = 5.496$	0.8
Ge	Ge (227)	$a = 5.6575$	RT [64]	$a = 5.572$	−1.5
H	H_2	d(H—H) = 0.7414	RT [64]	0.7422	0.1
He	α-He (194)	$a = 3.555$	4K [64]	$a = 3.556$	0.0
		$c = 5.798$		$c = 5.798$	0.0
Hf	Hf (194)	$a = 3.1946$	RT [64]	$a = 3.082$	−3.5
		$c = 5.0511$		$c = 4.961$	−1.8
Hg	HgTe (216)	$a = 6.4623$	RT [64]	$a = 6.585$	2.9
	HgS (216)	$a = 5.8517$	RT [64]	$a = 5.978$	2.6
	HgSe (216)	$a = 6.084$	RT [64]	$a = 6.211$	2.7
I	I_2	d(I—I) = 2.6663	RT [64]	2.657	−0.3
	LiI (225)	$a = 6.00$	RT [73]	$a = 6.000$	0.0
In	InAs (216)	$a = 6.0584$	RT [64]	$a = 6.181$	2.0
	InP (216)	$a = 5.8688$	RT [64]	$a = 5.949$	1.4
Ir	Ir (225)	$a = 3.8389$	RT [64]	$a = 3.857$	0.5
	$IrAl_3$ (194)	$a = 4.246$	RT [70]	$a = 4.200$	−1.1
		$c = 7.756$		$c = 7.618$	−1.8
K	K (229)	$a = 5.321$	RT [64]	$a = 5.311$	0.3
	KF (225)	$a = 5.33$	RT [64]	$a = 5.354$	0.5
Kr	KrF_2	d(Kr—F) = 1.89	RT [64]	1.916	1.4
La	La (194)	$a = 3.774$	RT [64]	$a = 3.824$	1.3
		$c = 12.171$		$c = 12.539$	3.0
	$LaTiO_3$ (62)	$a = 5.630$	10 K [83]	$a = 5.602$	−0.5
		$b = 5.584$		$b = 5.712$	2.2
		$c = 7.901$		$c = 7.899$	0.0
Li	Li (229)	$a = 3.5092$	RT [64]	$a = 3.450$	−1.7
	LiF (225)	$a = 4.018$	RT [64]	$a = 4.038$	0.5
Lu	Lu (194)	$a = 3.5052$	RT [64]	$a = 3.499$	−0.2
		$c = 5.5494$		$c = 5.490$	−1.0
	LuC_2 (87)	$a = 3.563$	RT [84]	$a = 3.611$	1.4
		$c = 5.964$		$c = 6.079$	1.9
Mg	Mg (194)	$a = 3.2094$	RT [64]	$a = 3.209$	0.0
		$c = 5.2105$		$c = 5.210$	0.0
	MgO (225)	$a = 4.2112$	RT [64]	$a = 4.277$	1.6
Mn	MnB_4 (12)	$a = 5.5029$	RT [85]	$a = 5.427$	−1.4
		$b = 5.3669$		$b = 5.278$	−1.4
		$c = 2.9487$		$c = 2.914$	−1.2
		$\beta = 122.71°$		$\beta = 122.37°$	−0.3

(Continued)

TABLE I
(Continued)

Element	Compound (space group number)	Structural parameters: Experiment	Temperature and reference	CASTEP	Error (%)
Mo	Mo (229)	$a = 3.147$	RT [64]	$a = 3.1588$	0.4
	$MoSi_2$ (139)	$a = 3.20$	RT [86]	$a = 3.195$	−0.1
		$c = 7.85$		$c = 7.791$	−0.8
N	N_2	d(N—N) = 1.0977	RT [64]	1.147	4.5
	ZrN (225)	$a = 4.62$	RT [64]	$a = 4.634$	0.3
Na	Na (229)	$a = 4.2906$	RT [64]	$a = 4.312$	0.5
	NaI (225)	$a = 6.462$	RT [64]	$a = 6.537$	1.2
Nb	Nb (229)	$a = 3.3004$	RT [64]	$a = 3.3153$	0.4
	NbO (221)	$a = 4.210$	RT [87]	$a = 4.2344$	0.6
Ne	Ne (225)	$a = 4.429$	4K [67]	$a = 4.380$	−1.1
Ni	Ni (225)	$a = 3.524$	RT [64]	$a = 3.500$	−0.7
	NiAs (186)	$a = 3.602$	RT [70]	$a = 3.549$	−1.5
		$c = 5.009$		$c = 5.031$	0.4
Np	NpAs (221)	$a = 3.31$	RT [88]	$a = 3.415$	3.2
O	O_2	d(O—O) = 1.217	RT [64]	1.230	1.1
Os	Os (194)	$a = 2.7344$	RT [89]	$a = 2.746$	0.4
		$c = 4.3173$		$c = 4.334$	0.4
	OsP_2 (58)	$a = 5.1012$	RT [90]	$a = 5.050$	−1.0
		$b = 5.9022$		$b = 5.889$	−0.2
		$c = 2.9183$		$c = 2.937$	0.6
P	P_2	d(P—P) = 1.8931	RT [64]	1.875	−0.9
Pb	Pb (225)	$a = 4.9502$	RT [64]	$a = 5.046$	1.9
	PbSe (225)	$a = 6.128$	RT [64]	$a = 6.151$	0.4
Pd	Pd (225)	$a = 3.8903$	RT [64]	$a = 3.903$	0.3
	PdSi (62)	$a = 5.610$	RT [91]	$a = 5.612$	0.0
		$b = 3.385$		$b = 3.354$	−0.9
		$c = 6.145$		$c = 6.153$	0.1
Po	α-Po (221)	$a = 3.345$	RT [70]	$a = 3.308$	−1.1
	YPo (225)	$a = 6.251$	RT [92]	$a = 6.288$	0.6
Pt	Pt (225)	$a = 3.9236$	RT [64]	$a = 3.971$	1.2
	PtS (131)	$a = 3.48$	RT [70]	$a = 3.515$	1.0
		$c = 6.11$		$c = 6.120$	0.2
Pu	PuO (225)	$a = 4.958$	RT [64]	$a = 5.006$	1.0
	PuS (525)	$a = 5.536$	RT [76]	$a = 5.525$	−0.2
Ra	Ra (229)	$a = 5.148$	RT [64]	$a = 5.288$	2.7
Rb	Rb (229)	$a = 5.705$	RT [64]	$a = 5.700$	−0.1
	RbBr (225)	$a = 6.877$	RT [93]	$a = 6.979$	1.5
Re	Re (194)	$a = 2.761$	RT [64]	$a = 2.758$	0.0
		$c = 4.458$		$c = 4.446$	−0.3
	Re_3B (63)	$a = 2.89$	RT [70]	$a = 2.889$	0.0
		$b = 9.313$		$b = 9.405$	1.0
		$c = 7.258$		$c = 7.235$	−0.3
Rh	Rh (225)	$a = 3.8032$	RT [64]	$a = 3.853$	1.3
	$RhTe_2$ (205)	$a = 6.448$	RT [94]	$a = 6.480$	0.5
Ru	Ru (194)	$a = 2.7058$	RT [64]	$a = 2.720$	0.5
		$c = 4.2816$		$c = 4.289$	0.2
	$RuAs_2$ (58)	$a = 5.4279$	RT [90]	$a = 5.340$	−0.6
		$b = 6.1834$		$b = 6.130$	0.0
		$c = 2.9685$		$c = 2.985$	0.9

(Continued)

TABLE I
(Continued)

Element	Compound (space group number)	Structural parameters: Experiment	Temperature and reference	CASTEP	Error (%)
S	S_2	d(S—S) = 1.8892	RT [64]	1.889	0.0
Sb	GaSb (216)	a = 6.0954	RT [64]	a = 6.132	0.6
	AlSb (216)	a = 6.1355	RT [64]	a = 6.078	−0.9
Sc	Sc (194)	a = 3.3088	RT [64]	a = 3.309	0.0
		c = 5.2680		c = 5.178	−1.7
	Sc_3In (194)	a = 6.421	RT [95]	a = 6.418	0.0
		c = 5.183		c = 5.183	0.0
Se	ZnSe (216)	a = 5.6676	RT [64]	a = 5.711	0.8
	BeSe (216)	a = 5.139	RT [64]	a = 5.194	1.1
Si	Si (227)	a = 5.4307	RT [64]	a = 5.440	0.2
	α-SiO_2 (152)	a = 4.902	13 K [96]	a = 4.987	1.7
		c = 5.400		c = 5.459	1.1
Sm	SmSe (196)	a = 6.159	RT [97]	a = 6.234	1.2
Sn	Sn (227)	a = 6.481	140 K [98]	a = 6.408	−1.1
	SnO_2 (136)	a = 4.736	RT [99]	a = 4.709	−0.6
		c = 3.185		c = 3.150	−1.1
Sr	Sr (225)	a = 6.0849	RT [64]	a = 6.085	0.0
	SrO (225)	a = 5.13	RT [64]	a = 5.17	0.9
Ta	Ta (229)	a = 3.303	RT [64]	a = 3.252	−1.5
	TaO (225)	a = 4.422	RT [100]	a = 4.490	1.5
Tc	Tc (194)	a = 2.738	RT [64]	a = 2.751	0.5
		c = 4.393		c = 4.392	0.0
	$TcOF_4$ (176)	a = 9.00	RT [101]	a = 9.220	2.4
		c = 7.92		c = 8.050	1.6
Te	Te (152)	a = 4.456	RT [64]	a = 4.437	−0.4
		c = 5.926		c = 5.900	−0.4
	ZnTe (216)	a = 6.101	RT [64]	a = 6.142	0.7
Th	ThN (225)	a = 5.167	RT [102]	a = 5.172	0.1
	ThO_2 (225)	a = 5.598	RT [103]	a = 5.578	−0.4
Ti	Ti (194)	a = 2.9506	RT [64]	a = 2.936	−0.5
		c = 4.6835		c = 4.658	−0.5
	Rutile TiO_2 (136)	a = 4.587	15 K [104]	a = 4.625	0.8
		c = 2.954		c = 2.965	0.4
Tl	Tl (194)	a = 3.4566	RT [64]	a = 3.595	4.0
		c = 5.5248		c = 5.544	0.3
	TlCl (221)	a = 3.835	RT [64]	a = 3.875	1.0
Tm	TmOI (129)	a = 3.887	RT [105]	a = 3.917	0.8
		c = 9.166		c = 9.175	0.1
	$CsTmCl_3$ (221)	a = 5.455	RT [106]	a = 5.457	0.0
U	UN_2 (225)	a = 5.31	RT [64]	a = 5.254	−1.1
	UC_2 (139)	a = 3.517	RT [107]	a = 3.524	0.2
		c = 5.987		c = 5.946	−0.7
V	V (229)	a = 3.024	RT [64]	a = 3.019	−0.2
	VN (225)	a = 4.137	RT [108]	a = 4.137	0.0
W	W (229)	a = 3.165	RT [64]	a = 3.222	1.8
	WC (187)	a = 2.906	RT [70]	a = 2.949	1.5
		c = 2.837		c = 2.873	1.3
Xe	XeF_2	d(Xe—F) = 1.977	RT [64]	2.030	2.7

(Continued)

TABLE I
(Continued)

Element	Compound (space group number)	Structural parameters: Experiment	Temperature and reference	CASTEP	Error (%)
Y	Y (194)	$a = 3.6482$	RT [64]	$a = 3.638$	−0.3
		$c = 5.7318$		$c = 5.672$	−1.0
	YF_3 (62)	$a = 6.354$	RT [109]	$a = 6.362$	0.1
		$b = 6.854$		$b = 6.903$	0.7
		$c = 4.395$		$c = 4.471$	1.7
Zn	Zn (194)	$a = 2.665$	RT [64]	$a = 2.641$	−0.9
		$c = 4.947$		$c = 4.865$	−1.7
	ZnS (216)	$a = 5.4193$	RT [64]	$a = 5.484$	1.2
Zr	Zr (194)	$a = 3.2316$	RT [64]	$a = 3.241$	0.3
		$c = 5.1475$		$c = 5.206$	0.6

Compressibility and Pressure-Induced Phase Transitions

One of the most important physical properties of inorganic crystals is their behavior under compression. Both the value of the bulk modulus and the phase stability of various polymorphs is of critical importance to, e.g., geophysics and mineral physics because experimental information on high-pressure behavior of minerals is rarely available.

BULK MODULUS AND EQUATION OF STATE

In quantum-mechanical total energy calculations, the bulk modulus and its pressure derivative are obtained by fitting an analytical equation of state (EOS) to either $E(V)$ or $P(V)$ curves. Such calculations for low-symmetry systems require the ability to optimize geometry at a fixed value of applied external pressure. The deviation of DFT-calculated bulk moduli from experimental values can be as large as 20% [110, 111]. Furthermore, the difference between LDA and GGA results can be quite substantial, partly due to the difference in the equilibrium unit-cell volume, which is generally underestimated in LDA calculations. High-quality theoretical determination of the EOS and of the bulk modulus requires sufficiently transferable pseudopotentials and well converged calculations with respect to the k-point sampling and the basis set size. With this proviso an agreement with experiment within a few percent can be achieved for a variety of materials: minerals (CaO [112], $CaSiO_3$ [113], $MgSiO_3$ [114], Mg_2SiO_4 [115], three polymorphs of silica [116]), metallic systems (Cu [117], Co and $CoSi_2$ [118], ε-FeSi [119], AlCo compounds [120]), and semiconductors (layered compounds GeS, GeSe, AsI_3 [121], nitride semiconductors [122], GaAs [123]).

Recent results on the compressibility of aluminosilicate garnets [124] provide a good illustration of the level of accuracy achievable with the PW-PP approach. These garnets crystallize in a body-centered cubic structure with 160 atoms per unit cell (although it is sufficient to use a primitive cell containing 80 atoms for the calculations). The structure can be described as consisting of chains in which corner-sharing SiO_4 tetrahedra and AlO_6 tetrahedra alternate. A third coordination polyhedron is a triangular dodecahedron occupied by metallic cations (e.g., Mg, Ca, Fe, or Mn). The compression mechanism for these materials is unclear from experimental data alone [125], and ab initio modeling is necessary to gain insight into the role of the cation in the structural changes under pressure. The compressibility of garnets depends only slightly on the identity of the metallic cation, and thus the required accuracy in the calculated bulk modulus is very high. Table II illustrates the level of agreement achieved using CASTEP: cell parameters are accurate to within 0.5%, and bulk moduli agree with experiment to 1–2%, so that the effect of the metallic cation on compressibility can be described quantitatively.

A detailed study of the polyhedra changes under pressure shows that the main compression mechanism in these compounds is the bending of the Si–O–Al angle between the octahedra and the tetra-

TABLE II

Calculated [124] and measured [125] lattice parameters, *a*, and bulk moduli, *B*, for aluminosilicate garnets. Percentage deviation of theoretical results from experiment is given in brackets.

		a (Å)	*B* (GPa)
Pyrope	Theory	11.395 (0.3)	170 ± 2 (0.6)
$Mg_3Al_2Si_3O_{12}$	Exp.	11.428	171 ± 2
Grossular	Theory	11.857 (0.1)	166 ± 2 (1.2)
$Ca_3Al_2Si_3O_{12}$	Exp.	11.848	168.4 ± 0.7
Almandine	Theory	11.509 (0.02)	176.5 ± 3.5 (0.9)
$Fe_3Al_2Si_3O_{12}$	Exp.	11.507	175 ± 7
Spessartine	Theory	11.616 (0.1)	183.4 ± 3.9 (2.5)
$Mn_3Al_2Si_3O_{12}$	Exp.	11.606	178.8 ± 0.8

hedra [124]. It can also be deduced that the increase of cation size in the sequence Mg–Fe–Mn does not change the qualitative characteristics of the compression process, and thus the increase of the bulk modulus in the pyrope–almandine–spessartine sequence is the "normal" trend in garnets. Cations as large as Ca cause excessive swelling of the structure which can be seen mainly as expansion and distortion of AlO_6 octahedra. This has the effect of lowering the bulk modulus of the structure and modifies the qualitative features of the compression process.

TEMPERATURE-INDUCED PHASE TRANSITIONS

DFT in the standard formulation is a zero-temperature method, and thus it is not straightforward to use this technique to study pressure–temperature or concentration–temperature phase diagrams. It is, however, possible to implement the Mermin functional [126], which is a generalization of the Kohn–Sham functional to finite temperatures. Alternatively, one can simply disregard electronic thermal effects at moderate temperatures.

The phase stability at finite temperatures can be studied directly using the variable cell shape molecular dynamics [127, 128]. This computationally very demanding technique has the advantage of being able to predict the stable structure at a given pressure and temperature based only on the number of fbrmula units per unit cell. It is not possible, however, to study metastable polymorphs using this approach.

Another viable computational option to bridge the gap between zero and finite temperature studies is to use a phonon description of solids. Investigations of this nature are quite rare because phonon calculations are computationally expensive. The most straightforward technique to calculate phonon spectra uses finite atomic displacements to calculate forces on atoms and thus to obtain the force constant matrix. If the range of the force constants is assumed to be short, as it typically is in parametrized force-model calculations, the entire dispersion relation can be evaluated from data taken from small ab initio calculations [129, 130]. The next step might be to calculate the vibrational entropy and thus the free energy in the quasiharmonic approximation. This approach was used to calculate, for example, the phase boundary for the orthorhombic–tetragonal transition in magnesium silicate perovskite [131]. The comparison of the calculated diagram with possible mantle geotherms showed that the tetragonal phase may be present in the lower mantle.

A more general and accurate method of phonon calculations is based on the linear response formalism [132, 133]. This technique uses the variational property of DFT to calculate the response of the system to small atomic displacements. The main advantage compared with the finite displacement method is that all calculations are performed with the primitive unit cell and no supercell calculations are required. This method has been successfully applied to several systems. The most notable success of this approach is the development of a model Hamiltonian using the lattice Wannier function formalism. This technique was used to study finite temperature ferroelectric phase transitions in systems such as the perovskite oxides $PbTiO_3$ [134] and $PbZrO_3$ [135] and the narrow-gap semiconductor Pb_3GeTe_4 [136].

Quantitative studies that predict transition temperatures based on lattice dynamics are still quite

rare. It is more common to extract qualitative information about structural instabilities and possible products of phase transformations from soft-mode analysis. For example, an ab initio study of phonon instabilities and coupling between modes in magnesium silicate perovskite revealed strongly unstable modes in cubic and tetragonal phases, which "freeze in" to ultimately form the orthorhombic phase [137]. Similarly, a pronounced soft mode was found at the X point in the cubic ZrO_2 structure, in agreement with the experimentally observed cubic to tetragonal phase transition [131].

PRESSURE-INDUCED PHASE TRANSITIONS

The quantum-mechanical approach has now become a routine way to study pressure-induced transitions. Both displacive and reconstructive types of phase transitions can be investigated by ab initio modeling techniques. Reconstructive transitions are best studied by constructing energy–volume curves for all possibly relevant space groups. The lowest energy structure at a given pressure then corresponds to the most stable modification at that pressure. Transition pressures and related volume changes can be obtained from the "common tangent" construction.

Reconstructive pressure-induced transitions have been studied in systems with various types of interatomic bonding. Recent examples include studies of the stability of the zincblende and cinnabar forms of ZnS [138], the transition from the low-pressure sodium chloride to the high-pressure cesium chloride structure in CaO [139], the isostructural semiconductor–semimetal phase transition in TiS_2 [140], the relative stability study of six phases in TiO_2 [141], and structural energetics of various alternative polymorphs of NbN [142]. A review of theoretical studies of exotic forms of tetrahedrally coordinated semiconductors is given in [143]. These unusual phases are synthesized as long-lived metastable forms of the elemental semiconductors silicon and germanium, and can also be produced in III–V semiconductors.

There have been a few attempts to study atomistic mechanisms of reconstructive phase transitions. Recent examples include the transformation path from graphite to diamond [144] and the calculation of fcc to bcc transitions in simple metals [145].

An example of the investigation of the origin and the driving force for displacive-type pressure-induced structural phase transition is the study of CsI under pressure [146]. The high-pressure phase

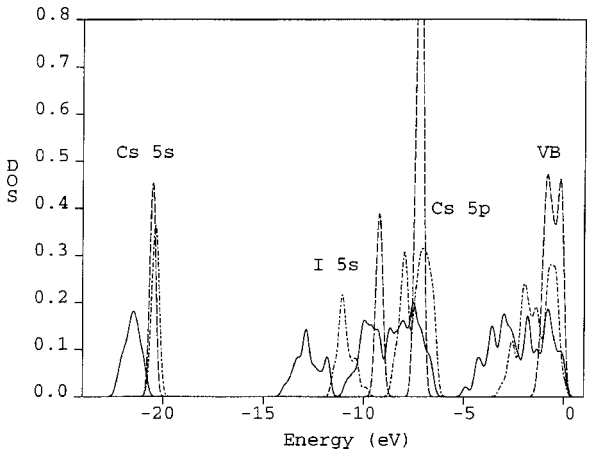

FIGURE 1. Pressure dependence of the density of electronic states (DOS) in CsI [146]: dashed line, 0 GPa; dash-dotted line, 25 GPa; solid line, 60 GPa. The 60 GPa data set corresponds to the high-pressure polymorph. Semicore states (Cs 5s, I 5s, Cs 5p) and valence band (VB) states (Cs 6s and I 5p) are shown.

of this compound has been the subject of some controversy, and ab initio calculations were used to demonstrate unambiguously that the structure of the high-pressure phase had a glide plane. It was shown by calculations that all structural parameters change discontinuously at the transition pressure, so the transition was of first order. Hexagonal distortions of the cubic phase that appear at the transition pressure have an electronic origin, as follows from an analysis of the electronic structure changes under pressure. It can be seen from Figure 1 that notionally inert core states of Cs (5s and 5p) and of I (5s) change their character under pressure—they broaden and eventually the Cs 5p peak overlaps with the I 5s states. This causes an overall change of the bonding character from largely ionic to covalent due to the hybridization between Cs 5p and I 5s states. The spatial distribution of Cs 5p states ceases to be spherical and these states take part in bonding in the high-pressure phase.

Another example of an added insight into the effect of pressure on electronic properties has been given in a study of the high-pressure phase of $CsGeCl_3$, where the calculations showed a change of the stereochemical activity of a lone electron pair under pressure from "active" to "inert," in agreement with the valence-shell electron-pair repulsion model [147].

PREDICTION OF NEW STRUCTURES AND THEIR PROPERTIES

Ab initio techniques can be successfully applied to study hypothetical or unknown structures. A simple example would be a study of a system that contains hydrogen atoms whose position cannot be unambiguously located using diffraction techniques. This is the case in, e.g., $CsHSO_3$, where experimental results were published without hydrogen positions. CASTEP calculations were subsequently used to find these positions and to predict structural and optical properties of this molecular compound under pressure [148]. This situation, where theoretical methods have an advantage over experiment, is typical for complex structures that contain hydrogen as well as heavy atoms.

Another type of poorly characterized structure is metastable polymorphs that often exist as high-pressure phases. For example, polymorphs of crystalline and amorphous carbon have long been the subject of experimental and theoretical studies that continue to discover new forms of carbon packing: nanotubes [149], carbon "onions" [150], etc. One structure that attracted some interest is supercubane, which was suggested to be a very dense polymorph. The structure of supercubane is not known accurately because the only source of experimental data comes from an electron diffraction study on a thin film. CASTEP calculations indicate that it is unlikely that supercubane has been observed yet [151]. Calculated structural properties at ambient conditions and under compression show that supercubane has a chemically sensible high-symmetry structure, but it is not a high-density polymorph at all.

Another carbon polymorph was predicted recently by combining a graph theoretical approach with density functional calculations [152]. The quotient graphs approach [153] was used to generate a number of trial structures that would topologically correspond to a framework structure of sp^2-carbon. These structures were further optimized using CASTEP, and their stability and electronic properties were studied. It was shown that there exists a nanoporous conducting framework structure of sp^2-hybridized carbon atoms that is relatively stable compared with other carbon polymorphs.

The graph theory approach [153], as well as the tiling of minimal surfaces scheme [154], can be useful tools for generating trial structures in the ab initio quest for new inorganic structures. There is a computationally more expensive alternative based on the Monte Carlo algorithm for packing of rigid fragments that was shown to be a successful way of determining crystal polymorphs of molecular crystals [155]. At present this approach has only been used with empirical interatomic force fields, in view of both computational effort required and insufficient validation work done in the area of DFT applications to molecular crystals. Recent successes of the DFT description of weakly bonded molecular crystals [148, 156–158] might induce an interest in a completely ab initio approach to polymorph prediction that would utilize a quantum-mechanical description of crystal bonding and would not use any a priori information about crystal symmetry. One should keep in mind, however, that the implementation of the Monte Carlo scheme [155] described above is presently not applicable to the polymorph prediction of framework structures.

Summary

We hope that this brief review has convinced the reader that the times have changed since a statement like, "It is impossible to calculate from first principles the details of crystal structures," [159] was generally accepted. The impact of quantum-mechanical modeling on such varied fields as materials science, inorganic crystallography, and molecular biology grows steadily, and it is safe to predict that its influence will continue to increase.

Despite the many successes, there remain a number of challenges. These include:

- Calculations for large systems containing thousands of atoms
- Higher computational speed to enable ab initio molecular dynamics simulations on large systems
- Higher accuracy in the prediction of total-energy-related properties such as molecular heats of formation, cohesive energies of solids, and energy hypersurfaces of chemical reactions including barrier heights
- Higher accuracy in the prediction of weak interactions (e.g., van der Waals energies)
- More accurate description of electronic excitations including energy band gaps in semiconductors
- More accurate calculation of a wider range of measurable properties such as NMR chemical shifts, infrared and Raman spectra, ultravio-

let/visible spectra, and photoemission spectra.

We are seeing steady progress addressing all of the above points. For example, research in linear-scaling (order-*N*) methods is progressing, but also the "traditional" PW-PP methods described in this article are constantly being improved. The treatment of systems with thousands of atoms is already possible and there is no fundamental obstacle to extending these methods even further. However, at a certain point it becomes questionable whether a full quantum-mechanical treatment of all atoms in a large model is really necessary, especially in cases such as reactions at specific catalytic sites. There is usually a crossover point where further increase in system size is not commensurate with the additional insight gained from fully ab initio calculations, and the development of hybrid schemes designed to address this issue will become more important.

ACKNOWLEDGMENTS

We are grateful to many colleagues for numerous stimulating discussions of the developments of density functional methods and of their applications to realistic problems, especially to Volker Heine, Erich Wimmer, and Mike Gillan. We would like to thank David Vanderbilt for making available his set of ultrasoft pseudopotentials codes, and Ming-Hsien Lee and Jyh-Shing Lin for their help with generation of ultrasoft potentials.

References

1. Hohenberg, P.; Kohn, W. Phys Rev B 1964, 136, 864.
2. Kohn, W.; Sham, L. J. Phys Rev A 1965, 140, 1133.
3. von Barth, U.; Hedin, L. J Phys C 1972, 5, 1629.
4. Gunnarsson, O.; Lunqvist, B. I.; Lunqvist, S. Solid State Commun 1972, 11, 149.
5. Perdew, J. P. Phys Rev B 1986, 33, 8822.
6. Becke, A. D. Phys Rev A 1988, 38, 3098.
7. Payne, M. C.; Teter, M. P.; Allen, D. C.; Arias, T. A.; Joannopolous, J. D. Rev Mod Phys 1992, 64, 1045.
8. Car, R.; Parrinello, M. Phys Rev Lett 1985, 55, 2471.
9. Gillan, M. J. J Phys 1989, 1, 689.
10. Rappe, A. K.; Rabe, K.; Kaxiras, E.; Joannopolous, J. D. Phys Rev B 1990, 41, 1227.
11. Lin, J. S.; Qteish, A.; Payne, M. C.; Heine, V. Phys Rev B 1993, 47, 4174.
12. Kleinman, L.; Bylander, D.M. Phys Rev Lett 1982, 48, 1425.
13. King-Smith, R. D.; Payne, M. C.; Lin, J. S. Phys Rev B 1991, 44, 13063.
14. Fischer, T. H.; Almlöf, J. J Phys Chem 1992, 96, 9768.
15. CASTEP Program. Molecular Simulations, Inc., San Diego, CA.
16. Stich, I.; Payne, M. C.; King-Smith, R. D.; Lin, J. S.; Clarke, L. J. Phys Rev Lett 1992, 68, 1351.
17. Stich, I.; Terakura, K.; Larson, B. E. Phys Rev Lett 1995, 74, 4491.
18. de Vita, A.; Stich, I.; Gillan, M. J.; Payne, M. C.; Clarke, L. J. Phys Rev Lett 1993, 71, 1276.
19. White, J. A.; Bird, D. M.; Stich, I.; Payne, M. C. Phys Rev Lett 1994, 73, 1404.
20. Gundersen, K.; Jacobsen, K. W.; Norskov, J. K.; Hammer, B. Surf Sci 1994, 304, 131.
21. White, J. A.; Bird, D. M.; Payne, M. C. Phys Rev B 1996, 53, 1667.
22. Gravil, P. A.; Bird, D. M. Surf Sci 1997, 377, 555.
23. Lindan, P. J. D.; Harrison, N. M.; Holender, J. M.; Gillan, M. J. Chem Phys Lett 1996, 261, 246.
24. Liu, F.; Mostoller, M.; Milman, V.; Chisholm, M. F.; Kaplan, T. Phys Rev B 1995, 51, 17192.
25. Kaplan, T.; Mostoller, M.; Chisholm, M. F. Phys Rev B 1998, 58, 12865.
26. Valladares, A.; White, J. A.; Sutton, A. P. Phys Rev Lett 1998, 81, 4903.
27. Perez, R.; Payne, M. C.; Stich, I.; Terakura, K. Phys Rev Lett 1997, 78, 678.
28. Bass, J. M.; Matthai, C. C. Phys Rev B 1997, 55, 13032.
29. Jarvis, M. R.; Perez, R.; van Bouwelen, F. M.; Payne, M. C. Phys Rev Lett 1998, 80, 3428.
30. Dawson, I.; Bristowe, P. D.; Lee, M. H.; Payne, M. C.; Segall, M. D.; White, J. A. Phys Rev B 1996, 54, 13723.
31. Maiti, A.; Chisholm, M. F.; Pennycook, S. J.; Pantelides, S. T. Phys Rev Lett 1996, 77, 1306.
32. Thomson, D. I.; Heine, V.; Finnis, M. W.; Marzari, N. Philos Mag Lett 1997, 76, 281.
33. Chisholm, M. F.; Maiti, A.; Pennycook, S. J.; Pantelides, S. T. Phys Rev Lett 1998, 81, 132.
34. Yan, Y.; Chisholm, M. F.; Duscher, G.; Maiti, A.; Pennycook, S. J.; Pantelides, S. T. Phys Rev Lett 1998, 81, 3675.
35. Molteni, C.; Francis, G. P.; Payne, M. C.; Heine, V. Phys Rev Lett 1996, 76, 1284.
36. Molteni, C.; Marzari, N.; Payne, M. C.; Heine, V. Phys Rev Lett 1997, 79, 869.
37. Pasteur, A. T.; Dixon-Warren, S. J.; Ge, Q.; King, D. A. J Chem Phys 1997, 106, 8896.
38. Hu, P.; King, D. A.; Crampin, S.; Lee, M. H.; Payne, M. C. J Chem Phys 1997, 107, 8103.
39. Szymanski, M. A.; Gillan, M. J. Surf Sci 1996, 367, 135.
40. Kantorovich, L. N.; Gillan, M. J. Surf Sci 1997, 376, 169.
41. Sandre, E.; Payne, M. C.; Gale, J. D. Chem Comm 1998, 22, 2445.
42. Stich, I.; Gale, J. D.; Terakura, K.; Payne, M. C. Chem Phys Lett 1998, 283, 402.
43. Andrews, S. B.; Burton, N. A.; Hiller, I. H.; Holender, J. M.; Gillan, M. J. Chem Phys Lett 1996, 261, 521.
44. Milman, V.; Lee, M. H. J Phys Chem 1996, 100, 6093.

45. Clark, S. J.; Ackland, G. J.; Crain, J. Europhys Lett 1998, 44, 578.
46. Clark, S. J.; Adam, C. J.; Cleaver, D. J.; Crain, J. Liquid Crystals 1997, 22, 477.
47. Segall, M. D.; Payne, M. C.; Boyes, R. N. Mol Phys 1998, 93, 365.
48. Segall, M. D.; Payne, M. C.; Ellis, S. W.; Tucker, G. T.; Boyes, R. N. Phys Rev E 1998, 57, 4618.
49. Clark, S. J.; Adam, C. J.; Hsueh, H. C.; Pu, F. N.; Crain, J. Mol Cryst Liquid Cryst 1997, 302, 433.
50. Wu, C. Q.; Fu, R. T.; Li, Z. Q.; Kawazoe, Y. J Phys 1997, 9, L351.
51. Gygi, F. Phys Rev B 1993, 48, 11692.
52. Hamann, D. R. Phys Rev B 1995, 51, 7337.
53. Gygi, F.; Galli, G. Phys Rev B 1995, 52, 2229.
54. Modine, N. A.; Zumbach, G.; Kaxiras, E. Phys Rev B 1997, 55, 10, 289.
55. Clarke, L. J.; Stich, I.; Payne, M. C. Comp Phys Commun 1992, 72, 14.
56. Pöykkö, S.; Puska, M. J.; Nieminen, R. M. Phys Rev B 1998, 57, 12, 174.
57. Kresse, G.; Furthmüller, J. Phys Rev B 1996, 54, 11, 169.
58. Vanderbilt, D. Phys Rev B 1990, 41, 7892.
59. Kresse, G.; Joubert, D. Phys Rev B 1999, 59, 1758.
60. Blöchl, P. E. Phys Rev B 1994, 50, 17, 593.
61. Louie, S. G.; Froyen, S.; Cohen, M. L. Phys Rev B 1982, 26, 1738.
62. Pulay, P. Chem Phys Lett 1980, 73, 393.
63. Hahn, T., Ed. International Tables for Crystallography; Kluwer Academic: Dordrecht, 1989.
64. Lide, D. R., Ed. CRC Handbook of Chemistry and Physics, 73rd ed.; CRC Press: Boca Raton, FL, 1993.
65. Sawada, H. Mater Res Bull 1994, 29, 127.
66. Zachariasen, W. H. Acta Crystallogr 1949, 2, 388.
67. Henshaw, D. G. Phys Rev 1958, 111, 1470.
68. Schifer, D.; Barrett, C. S. J Appl Crystallogr 1969, 2, 30.
69. Doerrscheidt, W.; Niess, N.; Schaefer, H. Z Naturforsch B 1976, 31, 890.
70. Hyde, B. G.; Andersson, S. Inorganic Crystal Structures; Wiley: New York, 1989.
71. Evers, J.; Oehlinger, G.; Sendlinger, B.; Weiss, A.; Schmidt, M.; Schramel, P. J Alloys Compounds 1992, 182, 175.
72. Downs, J. W.; Ross, F. K.; Gibbs, G. V. Acta Crystallogr Sect B 1985, 41, 425.
73. Zav'yalova, A. A.; Imamov, R. M. Zh Strukt Khim 1972, 13, 869.
74. Ott, H. Phys Z 1923, 24, 209.
75. Huang, Q.; Chmaissem, O.; Caponi, J. J.; Chaillout, C.; Marezio, M.; Tholence, J. L.; Santoro, A. Physica C 1994, 227, 1.
76. Zachariasen, W. H. Acta Crystallogr 1949, 2, 291.
77. Wolcyrz, M.; Kepinski, L. J Solid State Chem 1992, 99, 409.
78. Bertaut, F.; Blum, P. C R Hebd Seances Acad Sci 1950, 231, 626.
79. Jauch, W.; Schultz, A. J.; Heger, G. J Appl Crystallogr 1987, 20, 117.
80. Ghandehari, K.; Luo, H.; Ruoff, A. L.; Trail, S. S.; DiSalvo, F. J. Phys Rev Lett 1995, 74, 2264.
81. Restori, R.; Schawrzenbach, D. Acta Crystallogr Sect B 1986, 42, 201.
82. Batchelder, D. N.; Simmons, R. O. J Chem Phys 1964, 41, 2324.
83. Eitel, M.; Greedan, J. E. J Less-Common Met 1986, 116, 95.
84. Atoji, M. J Chem Phys 1961, 35, 1950.
85. Andersson, S. Acta Chem Scand 1969, 23, 687.
86. Tabata, H.; Hirano, T. J Jpn Inst Met 1988, 52, 1154.
87. Kubaschewski, O.; Hopkins, B. E. J Less-Common Met 1960, 2, 172.
88. Dabos, S.; Dufour, C.; Benedict, U.; Spirlet, J. C.; Pages, M. Physica 1986, 144, 79.
89. Finkel, V. A.; Palatnik, M. I.; Kovtun, G. P. Phys Met Metall 1971, 32, 231.
90. Kjekshus, A.; Rakke, T.; Andresen, A. F. Acta Chem Scand A 1977, 31, 253.
91. Goeransson, K.; Engstroem, I.; Nolaeng, B. J Alloys Comp 1995, 219, 107.
92. Prokin, E. S.; Ershova, Z. W.; Chebotarev, N. T.; Ermolajev, E. E. Izv Akad Nauk SSSR, Neorg Mater 1975, 11, 1230.
93. Ahtee, M. Ann Acad Sci Fenn Ser A6 Phys 1969, 313, 1.
94. Kjekshus, A.; Rakke, T.; Andresen, A. F. Acta Chem Scand A 1978, 32, 209.
95. Compton, V. B.; Matthias, B. T. Acta Crystallogr 1962, 15, 94.
96. Lager, G. A.; Jorgensen, J. D.; Rotella, F. J. J Appl Phys 1982, 53, 6751.
97. Guittard, M.; Benacerraf, A. C R Hebd Seances Acad Sci 1959, 248, 2589.
98. Lee, J. A.; Raynor, G. V. Nature 1954, 174, 1011.
99. Seki, H.; Ishizawa, N.; Mizutani, N.; Kato, M. J Ceram Soc Jpn 1984, 92, 219.
100. Steeb, S.; Renner, J. Metall 1967, 21, 93.
101. Edwards, A. J.; Jones, G. R.; Sills, R. J. C. J Chem Soc A 1970, 2521.
102. Gerward, L.; Olsen, J. S.; Benedict, U.; Itie, J.-P.; Spirlet, J. C. J Appl Crystallogr 1985, 18, 339.
103. Whitfield, H. J.; Roman, D.; Palmer, A. R. J Inorg Nucl Chem 1966, 28, 2817.
104. Burdett, J. K.; Hughbanks, T.; Miller, G. J.; Richardson, J. W.; Smith, J. V. J Am Chem Soc 1987, 109, 3639.
105. Kruse, F. H.; Asprey, L. B.; Morosin, B. Acta Crystallogr 1962, 14, 541.
106. Meyer, G. Naturwissenschaften 1978, 65, 258.
107. Rundle, R. E.; Baenziger, N. C.; Wilson, A. S.; McDonald, R. A. J Am Chem Soc 1948, 70, 99.
108. Kubel, F.; Flack, H. D.; Yvon, K. Phys Rev B 1987, 36, 1415.
109. Cheetham, A. K.; Norman, N. Acta Chem Scand A 1974, 28, 55.
110. Recio, J. M.; Blanco, M. A.; Luana, V.; Pandey, R.; Gerward, L.; Olsen, J. S. Phys Rev B 1998, 58, 8949.
111. D'Arco, P.; Fava, F. F.; Dovesi, R.; Saunders, V. R. J Phys 1996, 8, 8815.
112. Karki, B. B.; Crain, J. J Geophys Res 1998, 103, 12, 405.

113. Karki, B. B.; Crain, J. Geophys Res Lett 1998, 25, 2741.
114. Karki, B. B.; Stixrude, L.; Clark, S. J.; Warren, M. C.; Ackland, G. J.; Crain, J. Am Mineral 1997, 82, 635.
115. Brodholt, J.; Patel, A.; Refson, K. Am Mineral 1996, 81, 257.
116. Karki, B. B.; Warren, M. C.; Stixrude, L.; Ackland, G. J.; Crain, J. Phys Rev B 1997, 55, 3465.
117. Qteish, A. Phys Rev B 1995, 52, 14, 497.
118. Milman, V.; Lee, M. H.; Payne, M. C. Phys Rev B 1994, 49, 16, 300.
119. Qteish, A.; Shawagfeh, N. Solid State Commun 1998, 108, 11.
120. Ogut, S.; Rabe, K. M. Phys Rev B 1994, 50, 2075.
121. Hsueh, H. C.; Crain, J. Phys Status Solidi B 1999, 211, 365.
122. Pugh, S. K.; Dugdale, D. J.; Brand, S.; Abram, R. A. Semicond Sci Technol 1999, 14, 23.
123. Kelsey, A. A.; Ackland, G. J.; Clark, S. J. Phys Rev B 1998, 57, 2029.
124. Akhmatskaya, E. V.; Nobes, R. H.; Milman, V.; Winkler, B. Z Kristallogr 1999, 214, 808.
125. Geiger, C. A. An Investigation of the Microscopic Structural and the Macroscopic Physicochemical Properties of Aluminosilicate Garnets and Their Relationships. Habilitationschrift, Kiel University, 1996.
126. Mermin, D. Phys Rev A 1965, 137, 1441.
127. Wentzcovich, R. M.; Martins, J. L.; Allen, P. B. Phys Rev B 1992, 45, 11, 372.
128. Souza, I.; Martins, J. L. Phys Rev B 1997, 55, 8733.
129. Ackland, G. J.; Warren, M. C.; Clark, S. J. J Phys: Condens Matter 1997, 9, 7861.
130. Warren, M. C.; Ackland, G. J. Phys Chem Miner 1996, 23, 107.
131. Parlinski, K.; Li, Z. Q.; Kawazoe, Y. Phys Rev Lett 1997, 78, 4063.
132. Baroni, S.; Giannozzi, P.; Testa, A. Phys Rev Lett 1987, 58, 1861.
133. Gonze, X.; Allan, D. C.; Teter, M. P. Phys Rev Lett 1992, 68, 3603.
134. Rabe, K. M.; Waghmare, U. V. J Phys Chem Solids 1996, 57, 1397.
135. Waghmare, U. V.; Rabe, K. M. Ferroelectric 1997, 194, 135.
136. Cockayne, E.; Rabe, K. M. Phys Rev B 1997, 56, 7947.
137. Warren, M. C.; Ackland, G. J.; Karki, B. B.; Clark, S. J. Mineral Mag 1998, 62, 585.
138. Qteish, A.; AbuJafar, M.; Nazzal, A. J Phys 1998, 10, 5069.
139. Karki, B. B.; Crain, J. J Geophys Res 1998, 103, 12, 405.
140. Allan, D. R.; Kelsey, A. A.; Clark, S. J.; Angel, R. J.; Ackland, G. J. Phys Rev B 1998, 57, 5106.
141. Milman, V. In Properties of Complex Inorganic Solids; Plenum: New York, 1997; p. 19.
142. Ogut, S.; Rabe, K. M. Phys Rev B 1995, 51, 10, 443.
143. Grain, J.; Ackland, G. J.; Clark, S. J. Rep Progr Phys 1995, 58, 705.
144. Scandolo, S.; Bernasconi, M.; Chiarotti, G.; Focher, P.; Tosatti, E. Phys Rev Lett 1995, 74, 4015.
145. Sliwko, V. L.; Mohn, P.; Schwarz, K. H.; Blaha, P. J Phys 1996, 8, 799.
146. Winkler, B.; Milman, V. J Phys 1997, 9, 9811.
147. Winkler, B.; Milman, V.; Lee, M. H. J Chem Phys 1998, 108, 5506.
148. Griewatsch, C.; Winkler, B.; Milman, V.; Pickard, C. J. Phys Rev B 1998, 57, 4321.
149. Charlier, J. C.; de Vita, A.; Blase, X.; Car, R. Science 1997, 275, 646.
150. de Heer, W. A.; Ugarte, D. Chem Phys Lett 1993, 207, 480.
151. Winkler, B.; Milman, V. Chem Phys Lett 1998, 293, 284.
152. Winkler, B.; Pickard, C. I.; Milman, V.; Klee, W. E.; Thimm, G. Chem Phys Lett 1999, 312, 536.
153. Bader, M.; Klee, W. E.; Thimm, G. Z Kristallogr 1997, 212, 553.
154. Mackay, A. L.; Terrones, H. Nature 1991, 352, 762.
155. Verwer, P.; Leusen, F. J. J. In Reviews in Computational Chemistry; Wiley: New York, 1998; Vol. 12, p. 325.
156. Chall, M.; Winkler, B.; Milman, V. J Phys 1996, 8, 9049.
157. Meijer, E. J.; Sprik, M. J Chem Phys 1996, 105, 8684.
158. Ikeda, T.; Sprik, M.; Terakura, K.; Parrinello, M. Phys Rev Lett 1998, 81, 4416.
159. Baur, W. H. Phys Chem Mineral 1977, 2, 3.